Method for estimating rockfall failure probability using photogrammetry

# Method for estimating rockfall failure probability using photogrammetry



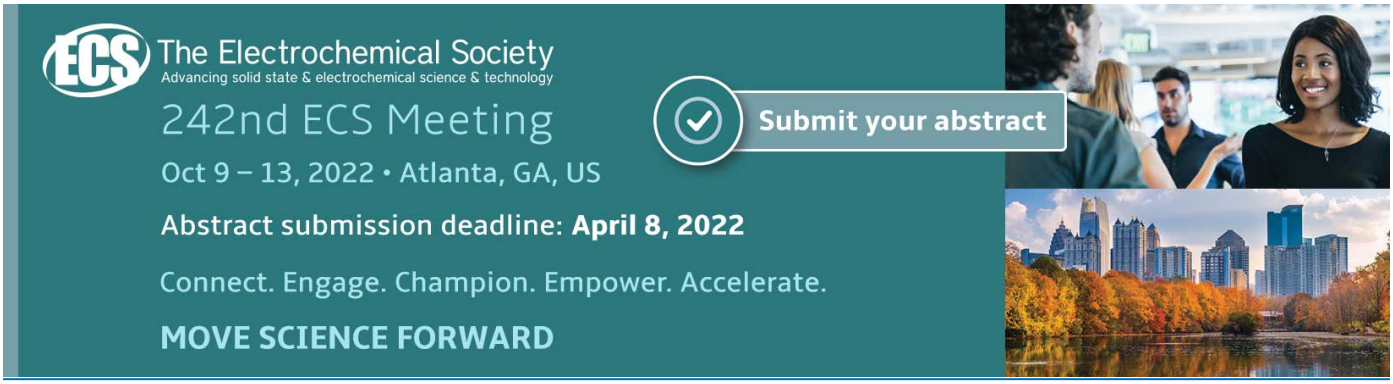

# Method for estimating rockfall failure probability using photogrammetry

**L Uotinen[1], M Janiszewski[1], R Mishra[1], H Munukka[1], M Szydlowska[1], D Martinelli[2] and P Dabove[2]**

[1]Fractuscan Ltd, Finland
[2]Politechnico di Torino, Italy

lauri.uotinen@aalto.fi

**Abstract**. Passageways cut through rock might be subjected to rockfalls. If a falling rock reaches the road area, the consequences can be disastrous. The traditional rockfall risk assessment method and risk mitigation are based on on-site investigations performed by a geologist or a rock engineer. The parameters resulting from the investigation, such as discontinuities, orientations and spacings, potential rockfall initiation locations, slope geometry, and ditch profile, are either measured or estimated. We propose a photogrammetry-based method for estimating the probability of failure for rockfall. Several photographs of the rock-cut are taken, and a 3D geometry is computed using photogrammetry. This model already allows remote visual inspection of the site. The information about joint planes can be discovered semiautomatically from the point cloud. Next, the probability of rockfall reaching the road area is computed using probabilistic kinematic analysis on the geometry extracted using photogrammetry. The results can be used to define the rockfall probability for each rock-cut. Furthermore, the results can be used to determine the appropriate rockfall risk mitigation actions for each rock-cut.

## 1. Introduction

Falling rocks are a significant risk across all continents [1-4]. Rockfall is a life-threatening hazard for highways, railroads, water passages, and open-pit mines. Rockfall risk assessment is a significant problem because of the vast amounts of assets and the considerable size of each asset. Currently, the risk assessment is carried out empirically based on visual inspections and expert judgement or using simplified analyses with visually obtained data. The subjective process is slow and prone to human errors. Imprecise risk assessment leads to overly conservative designs that are expensive and dangerous, could threaten life and cause economic or ecological problems.

The state-of-the-art technology is to use remote sensing technologies to map rock-cuts to assess rockfall risk [5-16]. The technology and associated software for rapid collection of initial data suitable for rockfall risk assessment already exists and has become a mature and reliable source for initial data for more advanced rockfall analyses [9, 17-21]. Finally, work to codify the automated design processes is already underway [22-24].

In this paper, we describe a method to assess the rockfall risk potential. The method is based on visually identifying kinematically admissible rock blocks from a 3D model generated with drone photogrammetry. A cross-section is then extracted and a probabilistic kinematic rockfall analysis is conducted. The probability of failure (PoF) is defined as the fraction of rocks that reach the road area divided with all possibilities. The factor of safety (FoS) is defined as the ratio of the distance-to-road

and the median-distance the trajectories reach. Using these, the PoF and FoS, the remedial measures can be planned for each identified risk.

In a previous pilot project, rock-cuts near main road 51 were located and a preliminary risk mapping was carried out on a 26 km long section. The section contained 72 cuts, of which three rock-cuts could be identified as high-risk sites, and another three cuts were identified as requiring more precise methods. In autumn 2020, in one of the identified high-risk cuts, a rockfall occurred and blocked one lane and damaged three cars. No personnel injuries were suffered. This rock-cut is shown in this paper as the example site and the back-calculation of the accident causing rockfall is also included.

Drone-based photogrammetry and the use of generated 3D models allow for a detailed investigation of the rock-cuts without access limitations and safety risks [25]. Precise measurements, marking potentially dangerous rock blocks and creating an overview of the rockfall probability in the model create a very useful decision-making database. The digital database can be used to design actions and measures such as reinforcement plans and maintenance plans. The creation of the database helps to manage the rockfall risks, to access them at any time and to track changes over time, to design a preventive course of actions instead of dealing with consequences of potentially costly, life-threatening events like rockfalls.

## 2. Methods

### *2.1. Site description*

The site is 361 m long and at maximum 22 m high rock-cut in Southern Finland. It is facing north on the south side of a motorway (figure 1). Three predominant naturally occurring joint sets were identified using photogrammetry-based extraction of discontinuity sets (tables 1 and 2). The Density column in table 2 is the Kernel Density Estimation and the percentage value represents how large portion of the observations fit to each joint sets.

### *2.2. Drone photogrammetry*

The rock-cuts were captured using DJI Phantom 4 Pro camera drone. The camera was set to take JPEG formatted images at 3-second intervals while the drone was flown along the rock-cut, capturing a set of overview images (Figure 2a) and a set of detail images (Figure 2b). Since the drone was moved continuously, shutter priority mode with 1/320 second shutter speed was used to avoid motion blur. The overview set is intended to capture the rough geometry of the whole area from the middle of the road to the top of the rock-cut. The overview set consists of three flight passes along rock-cut where the distance to the ground surface was 20 to 40 meters.

The detailed set was captured at a 7 to 15 m distance to the surface and the number of flight passes was 3 to 6 depending on the height of the rock-cut. This set is intended to capture detailed geometry of the rock-cut, which should allow for the detection of joint planes, fractures, and loose blocks. For safety reasons, flying the drone above or close to the road was avoided; thus, the detailed images could not be taken around the toe of the rock-cut. In any case, image capturing positions and orientations were so that 70 % overlap is achieved between images of adjacent flight passes.

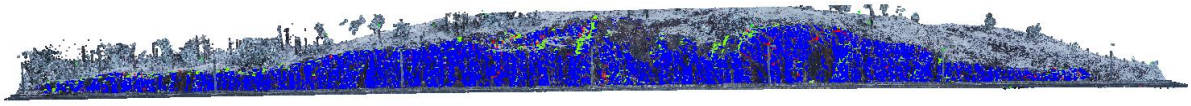

**Figure 1**. The inspected rock-cut. The blue color indicates the blast surface.

**Table 1.** Orientation of the three natural joint directions identified.

| DS | Dip direction (º) | Dip (º) | Density | % |
|---|---|---|---|---|
| $J_1$ | 213 | 85 | 0.2746 | 18.26 |
| $J_2$ | 72 | 67 | 0.1054 | 2.61 |
| $J_3$ | 223 | 44 | 0.0979 | 1.30 |

**Table 2.** Spacing of the joints identified.

| DS | Spacing (Sn) non persistent (m) | Min | Max | Standard deviation | Spacing (Sn) full persistent (m) | Min | Max | Standard deviation |
|---|---|---|---|---|---|---|---|---|
| $J_1$ | 0.41 | 0.01 | 6.42 | 0.36 | 0.13 | 0.01 | 1.42 | 0.14 |
| $J_2$ | 1.67 | 0.02 | 18.65 | 2.39 | 1.23 | 0.01 | 18.65 | 2.21 |
| $J_3$ | 1.65 | 0.01 | 10.01 | 1.99 | 1.00 | 0.01 | 9.85 | 1.60 |

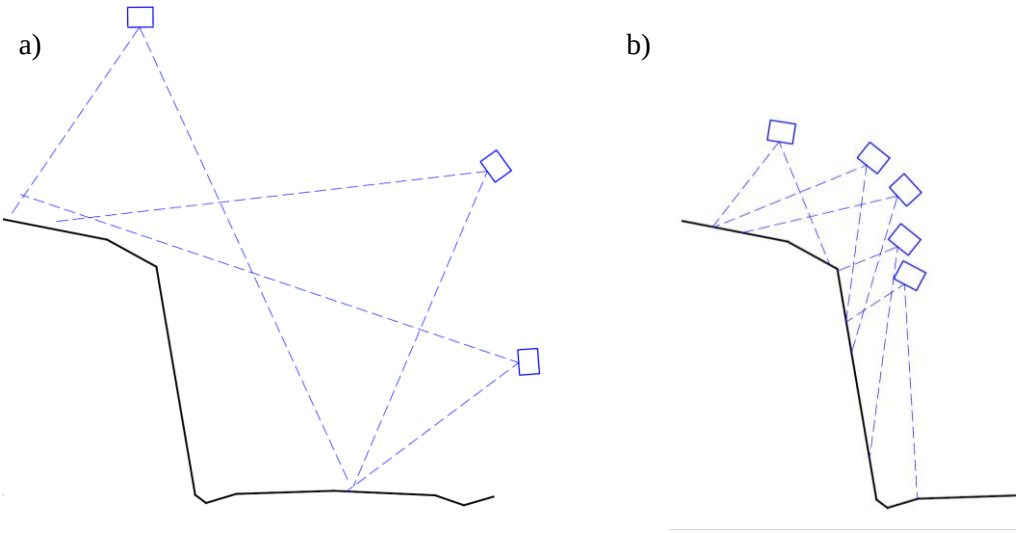


**Figure 2.** Camera drone image capturing positions for the overview image set (a) and the detail images set (b).

**Table 3.** Image pre-processing settings in Adobe Lightroom Classic.

| Pre-processing step | Develop settings | Value set |
|---|---|---|
| Delighting | Shadows | +100 |
| | Highlights | -100 |
| | Clarity | +20 |
| Deconvolution Sharpening | Amount | 50 |
| | Radius | 0.5 |
| | Detail | 100 |

### *2.3. Post-processing*

The drone images were pre-processed in photo editing software Adobe Lightroom Classic v. 10.1.1 in two steps. First, the images were delighted to even out the lighting by increasing the brightness of the shadow areas and decreasing brightness in overexposed areas. Delighting helps achieve a more consistent quality of the final model that is easier to interpret [26]. Second, the sharpness of the images was increased using the deconvolution sharpening method. The modified parameters and their values are given in table 3.

### *2.4. Photogrammetric reconstruction*

The 3D models of the rock-cuts were reconstructed using RealityCapture photogrammetry software. The processed drone images were imported and aligned using default settings. The resulting component consisted of 707 images. Next, the model was reconstructed in Normal settings and colorized. The point cloud was exported as a .xyz file and imported into CloudCompare for visual identification of the risks.

### *2.5. Visual identification of risks*

The visual identification of risks was made with the help of identified fracture planes. Rock blocks were sought out where three or more rock joints meet. Plane fitting and joint tracing tools were used to extend the length of fracture surfaces to see if they can create a kinematically admissible block. The shape and size of the blocks were measured for further analysis. The rock-cut was also inspected for toppling rock, sliding rock, wedges, weakness zones in addition to rockfall risks.

## 3. Results and discussion

### *3.1. Visually identified risks in the rockfall*

In total, eight geotechnical risks were visually observed, of which four (P1, P3, P5, P8) were rockfall risks, two wedges (P2, P6), and (P4) was the location of the already occurred rockfall used for back-analysis. There is also one place where sliding could occur (P7) (figure 3 and table 4).

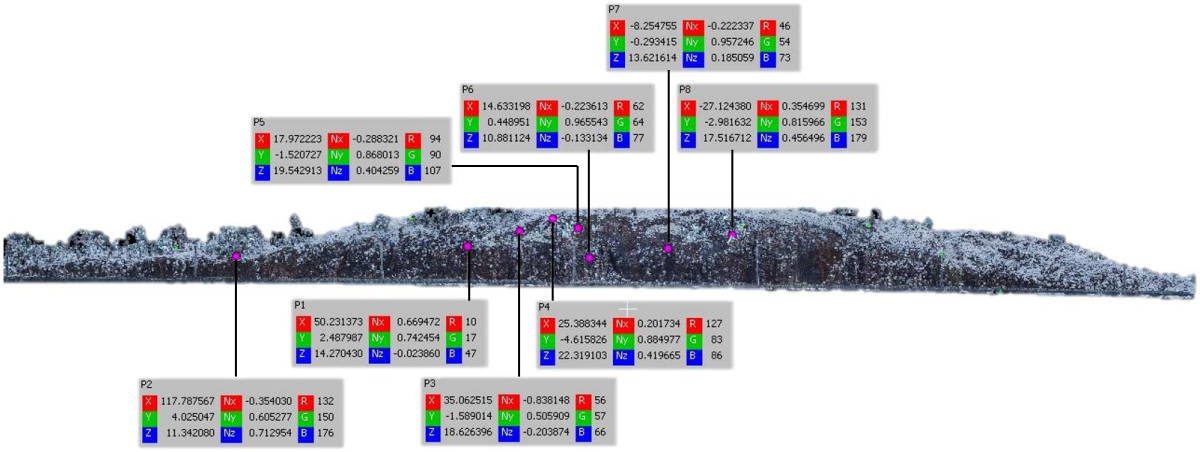


**Figure 3.** Locations of the visual observations P1-P8 with relative coordinates, normal vectors and RGB color values of the picked point.

**Table 4.** Picture of each observation P1-P8.

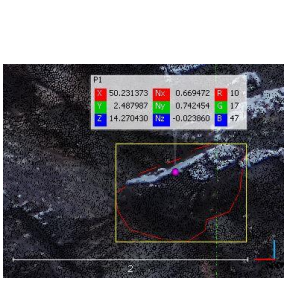
P1 rockfall risk

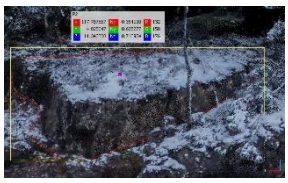
P2 wedge risk

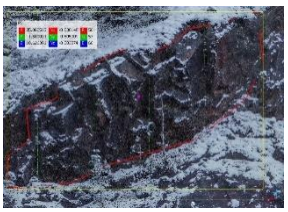
P3 rockfall risk

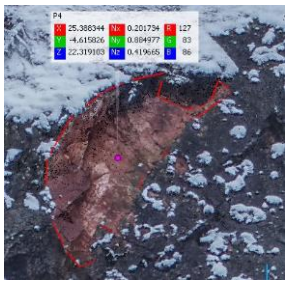
P4 back-calculation

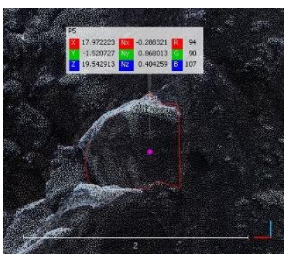
P5 rockfall risk

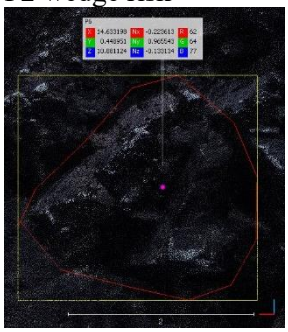
P6 wedge risk

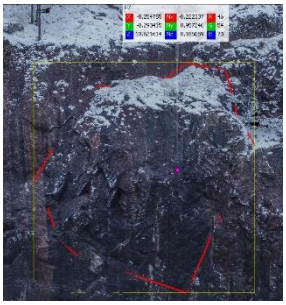
P7 sliding risk

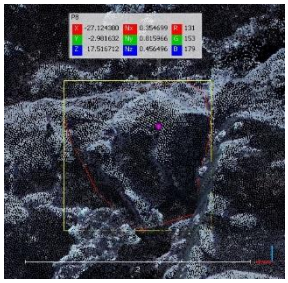
P8 rockfall risk

### *3.2. Kinematic rockfall simulations*

Photogrammetry was used to measure the block size and the 2D cross section extracted at each potential rockfall location, a kinematic rockfall analysis was conducted using the Roscience RocFall software with 10 000 trajectories. The probability of detachment was not considered. The initial horizontal velocity was simulated using a normal distribution with mean of 0.3 m/s and standard deviation of 0.1 m/s. The material parameters rock bedrock, soil and asphalt are shown in Table 5. The resulting trajectories histograms are shown in Table 6. Then the Probability of Failure (PoF) and the Factor of Safety (FoS) were calculated from the histograms and the results are shown in Table 7. The definitions for PoF and FoS are

PoF = (number of trajectories reaching at least the edge of the road) / (number of all trajectories)
FoS = (horizontal distance between the initiation point and the edge of road) /
(median, or 50 % fractile, of the horizontal distance flown).

### *3.3. Discussion of the results*

In the preceding remote inspection with no site visit associated, the highest cross-section of the rock-cut received PoF = 54.7 % and FoS = 1.16 and the nearest-to-road cross-section received PoF = 99.9 % and FoS = 0.39. The site visit allows a much more accurate representation of the unevenness of the rock-cut and the quality is sufficient to visually identify potential loose blocks. The unevenness causes bounces which may lead to the road area, as indicated in Table 3. As the location of the potentially dangerous blocks has been indicated, the threat may be dealt with by either rock reinforcement or removal of the threat.

Considering the back-analysis of the occurred rockfall (observation P4), a similar result is obtained and most of the rock trajectories are reaching the lane closest to the rock-cut. Interestingly, the PoF is relatively low 10 % and the FoS is reasonably high 1.15. The damage coincides with the first nights with freezing temperatures, which suggests that the freeze-thaw phenomenon is one possible mechanism why the rockfall occurred.

**Table 5.** Material properties used in the kinematic rockfall simulations.

| Material | Colour | Normal Restitution | Tangential Restitution | Friction Angle |
|---|---|---|---|---|
| Bedrock | | Normal distribution<br>Mean: 0.5<br>Std dev: 0.04<br>Rel. Min: 0.12<br>Rel. Max: 0.12 | Normal distribution<br>Mean: 0.9<br>Std dev: 0.03<br>Rel. Min: 0.09<br>Rel. Max: 0.09 | 30 |
| Soil | | Normal distribution<br>Mean: 0.25<br>Std dev: 0.04<br>Rel. Min: 0.12<br>Rel. Max: 0.12 | Normal distribution<br>Mean: 0.75<br>Std dev: 0.03<br>Rel. Min: 0.09<br>Rel. Max: 0.09 | 30 |
| Asphalt | | Normal distribution<br>Mean: 0.4<br>Std dev: 0.04<br>Rel. Min: 0.12<br>Rel. Max: 0.12 | Normal distribution<br>Mean: 0.9<br>Std dev: 0.03<br>Rel. Min: 0.09<br>Rel. Max: 0.09 | 30 |

**Table 6.** The trajectories on left and resulting histogram on right for the rockfalls P1, P3, P4, P5, P8.

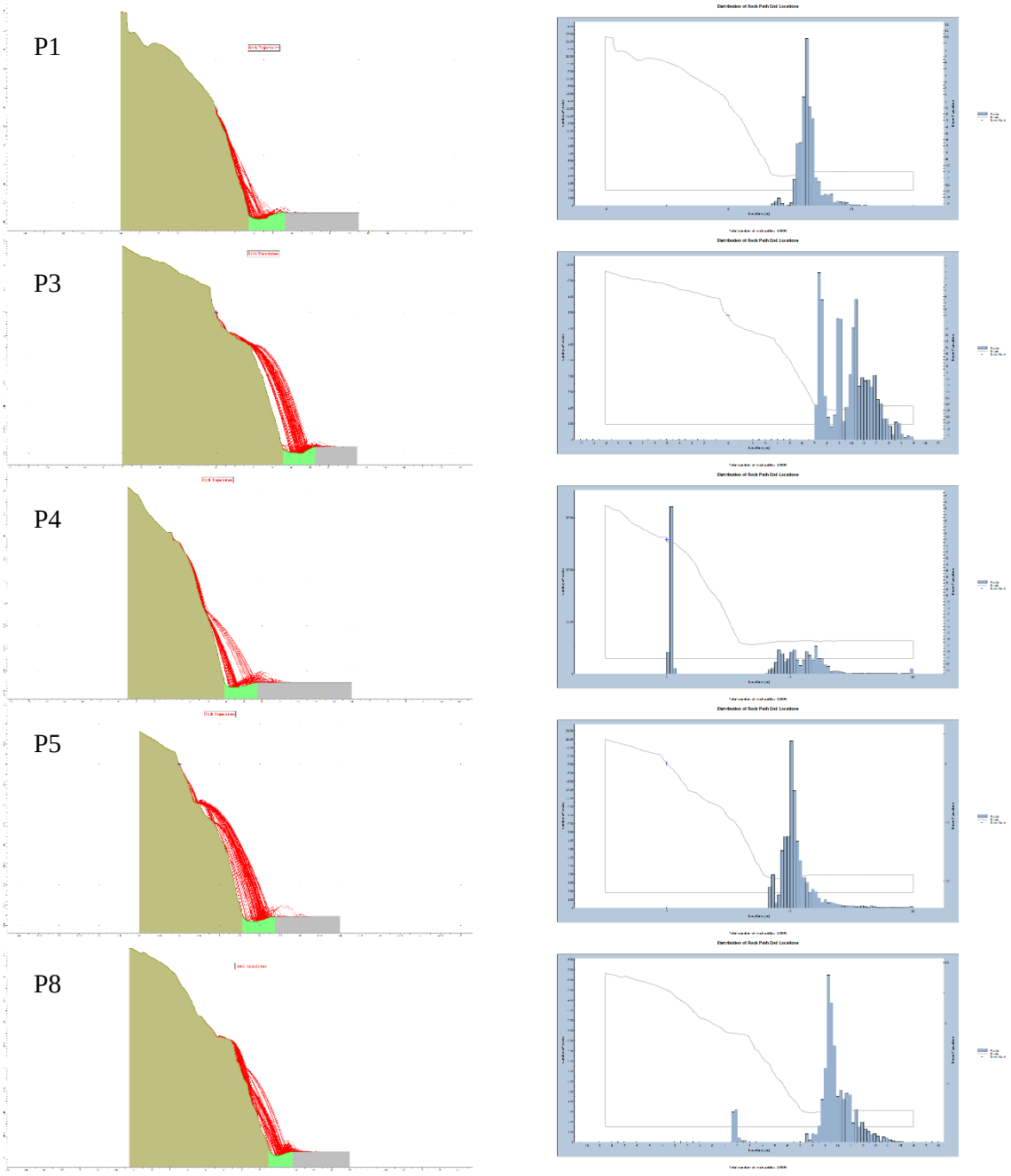


**Table 7.** The factor of safety and probability of failure for the rockfalls P1, P3, P4, P5, P8.

| Observation | Type | FoS | PoF |
|---|---|---|---|
| P1 | rockfall risk | 1.15 | 11.7 % |
| P3 | rockfall risk | 1.12 | 33.7 % |
| P4 | back-calculation | 1.15 | 9.9 % |
| P5 | rockfall risk | 1.00 | 50.0 % |
| P8 | rockfall risk | 1.02 | 47.4 % |

## 4. Conclusion

The proposed method creates photorealistic high-resolution 3D models, which allow safe visual inspection of rock-cuts to locate hazards and digital measurements of the shape, orientation, and dimensions of the blocks identified as potentially unstable. Considering rockfall hazard, four kinematically admissible blocks were selected for analysis using probabilistic kinematic analysis. The results are similar to the earlier preliminary remote results but more precise by detecting the potential rockfall locations. The rock surface geometry is considerably more accurate, enabling a more accurate rockfall trajectory analysis as the bounces from the rock-cut can be analyzed. Simulated trajectories with bounces from the rock-cut were present in all of the analyzed cross-sections.

## Acknowledgments

The authors gratefully acknowledge the Finnish Transport Infrastructure Agency Väylävirasto for funding the work.

## References

[1] Guzzetti F, Reichenbach P and Wieczorek G F 2003 Rockfall hazard and risk assessment in the Yosemite Valley, USA *Nat. Hazards Earth Syst. Sci.* **3** pp 491–503
[2] Budetta P 2004 Assessment of rockfall risk along roads *Nat. Hazards Earth Syst. Sci.* **4** pp 71–81
[3] Agliardi F, Crosta G B and Frattini P 2009 Integrating rockfall risk assessment and countermeasure design by 3D modelling techniques *Nat. Hazards Earth Syst. Sci.* **9** p 1059
[4] Wang X, Frattini P, Crosta G B, Zhang L, Agliardi F, Lari S and Yang Z 2014 Uncertainty assessment in quantitative rockfall risk assessment *Landslides* **11** pp 711–22
[5] Piras M, Taddia G, Forno M G, Gattiglio M, Aicardi I, Dabove P, Lo Russo S and Lingua A 2017 Detailed geological mapping in mountain areas using an unmanned aerial vehicle: application to the Rodoretto Valley, NW Italian Alps *Geomatics, Nat. Hazards and Risk* **8** pp 137–49
[6] Lato M, Hutchinson D J, Harrap R, Diederichs M S and Ball D 2009 Engineering monitoring of rockfall hazards along transportation corridors: using mobile terrestrial LiDAR. *Nat. Hazards Earth Syst. Sci.* **9** pp 935–46
[7] Lato M J, Hutchinson D J, Gauthier D, Edwards T and Ondercin M 2014 Comparison of airborne laser scanning, terrestrial laser scanning, and terrestrial photogrammetry for mapping differential slope change in mountainous terrain *Canadian Geotechnical J. **52** pp* 129–40.
[8] Crosta G B, Agliardi F, Frattini P and Lari S 2015 Key issues in rock fall modeling, hazard and risk assessment for rockfall protection *Engineering Geology for Society and Territory* ed G Lollino et al. (Cham: Springer) vol 2 pp 43–58
[9] Budetta P D L C, De Luca C and Nappi M 2016 Quantitative rockfall risk assessment for an important road by means of the rockfall risk management (RO. MA.) method *Bull. Eng. Geol. Env.* **75** pp 1377–97
[10] Fanos A M, Pradhan B, Aziz A A, Jebur M N and Park H J 2016 Assessment of multi-scenario rockfall hazard based on mechanical parameters using high-resolution airborne laser scanning data and GIS in a tropical area *Env. Earth Sci.* **75** p 1129
[11] Mineo S, Pappalardo G, D'urso A and Calcaterra D 2017 Event tree analysis for rockfall risk assessment along a strategic mountainous transportation route *Env. Earth Sci.* **76** p 620
[12] Saroglou C, Asteriou P, Zekkos D, Tsiambaos G, Clark M and Manousakis J 2018 UAV-based mapping, back analysis and trajectory modeling of a coseismic rockfall in Lefkada island, Greece *Nat. Hazards Earth Syst. Sci.* **18** pp 321–33
[13] Sarro R, Riquelme A, García-Davalillo J, Mateos R, Tomás R, Pastor J and Herrera G 2018 Rockfall simulation based on uav photogrammetry data obtained during an emergency declaration: Application at a cultural heritage site. *Remote Sens.* **10** p 1923
[14] Liu C, Liu X, Peng X, Wang E and Wang S 2019 Application of 3D-DDA integrated with unmanned aerial vehicle–laser scanner (UAV-LS) photogrammetry for stability analysis of a blocky rock mass slope *Landslides* **16** pp 1645–61

[15] Vanneschi C, Camillo M D, Aiello E, Bonciani F and Salvini R 2019 SfM-MVS Photogrammetry for Rockfall Analysis and Hazard Assessment Along the Ancient Roman Via Flaminia Road at the Furlo Gorge *ISPRS Int. J. Geo-Inf.* **8** p 325
[16] Williams C, Morkeh J, Dorfschmidt K, Poon C, Matlashewski P and Carvalho J 2019 Innovative Rockfall Solutions Based on Calibration and Field Testing *Mining, Metallurgy & Exploration*, **37** pp 101–16
[17] Dunham L, Wartman J, Olsen M J, O'Banion M and Cunningham K 2017 Rockfall Activity Index (RAI): A lidar-derived, morphology-based method for hazard assessment *Eng. Geol.* **221** pp 184–92
[18] Kromer R, Lato M, Hutchinson D J, Gauthier D and Edwards T 2017 Managing rockfall risk through baseline monitoring of precursors using a terrestrial laser scanner *Canadian Geotech. J.* **54** pp 953–67
[19] Kromer R A, Rowe E, Hutchinson J, Lato M and Abellán A 2018 Rockfall risk management using a pre-failure deformation database *Landslides* **15** pp 847–58
[20] Fanos A M and Pradhan B 2019 A novel rockfall hazard assessment using laser scanning data and 3D modelling in GIS *Catena* **172** pp 435–50
[21] Carlà T, Nolesini T, Solari L, Rivolta C, Dei Cas L and Casagli N 2019 Rockfall forecasting and risk management along a major transportation corridor in the Alps through ground-based radar interferometry *Landslides* **16** pp 1425–35
[22] Abdulai M and Sharifzadeh M 2019 Uncertainty and Reliability Analysis of Open Pit Rock Slopes: A Critical Review of Methods of Analysis *Geotech. Geol. Eng.* **37** pp 1223–47
[23] Bozorgzadeh N and Harrison J P 2019 Reliability-based design in rock engineering: application of Bayesian regression methods to rock strength data *J. Rock Mech. Geotech. Eng* **11** pp 612–27
[24] Spross J, Stille H, Johansson F and Palmstrøm A 2019 Principles of risk-based rock engineering design *Rock Mech. Rock Eng.* **53** pp 1129–43
[25] Uotinen L, Janiszewski M, Baghbanan A, Caballero-Hernandez E, Oraskari J, Munukka H, Szydlowska M and Rinne M 2019 Photogrammetry for recording rock surface geometry and fracture characterization *Rock Mechanics for Natural Resources and Infrastructure Development - Full Papers: Proceedings of the 14th International Congress on Rock Mechanics and Rock Engineering (ISRM 2019), September 13-18, 2019, Foz do Iguassu, Brazil* ed S A B da Fontura, R J Rocca and J P Mendoza (London: CRC Press) pp 461–68
[26] Janiszewski, M., Uotinen, L., Baghbanan, A., & Rinne, M. (2020). Digitisation of hard rock tunnel for remote fracture mapping and virtual training environment. In C. C. Li, H. Ødegaard, A. H. Høien, & J. Macias (Eds.), *ISRM International Symposium - EUROCK 2020: International Society for Rock Mechanics and Rock Engineering Norwegian Group for Rock Mechanics* Norsk Betongforening